







## RESEARCH ARTICLE

# Structural characterization of $\beta$ -propiolactone inactivated severe acute respiratory syndrome coronavirus 2 (SARS-CoV-2) particles

Dmitry V. Bagrov<sup>1,2</sup>  | Grigory S. Glukhov<sup>1</sup> | Andrey V. Moiseenko<sup>1,3</sup> |  
Maria G. Karlova<sup>1</sup> | Daniil S. Litvinov<sup>1</sup> | Petr A. Zaitsev<sup>1</sup> |  
Liubov I. Kozlovskaya<sup>4,5</sup>  | Anna A. Shishova<sup>4,5</sup> | Anastasia A. Kovpak<sup>4</sup> |  
Yury Y. Ivin<sup>4</sup> | Anastasia N. Pinaeva<sup>4</sup> | Alexey S. Oksanich<sup>6</sup> | Viktor P. Volok<sup>1,4</sup> |  
Dmitry I. Osolodkin<sup>2,4,5</sup>  | Aydar A. Ishmukhmetov<sup>4,5</sup>  | Alexey M. Egorov<sup>1,3,6</sup> |  
Konstantin V. Shaitan<sup>1,3</sup>  | Mikhail P. Kirpichnikov<sup>1</sup> | Olga S. Sokolova<sup>1,7</sup> 

<sup>1</sup>Faculty of Biology, Lomonosov Moscow State University, Moscow, Russia

<sup>2</sup>Faculty of Chemistry, Lomonosov Moscow State University, Moscow, Russia

<sup>3</sup>N. N. Semenov Federal Research Center for Chemical Physics, Russian Academy of Sciences, Moscow, Russia

<sup>4</sup>Chumakov Federal Scientific Center for Research and Development of Immune-and-Biological Products of Russian Academy of Sciences (Institute of Poliomyelitis), Moscow, Russia

<sup>5</sup>Institute of Translational Medicine and Biotechnology, Sechenov First Moscow State Medical University, Moscow, Russia

<sup>6</sup>Mechnikov Research Institute of Vaccines and Sera, Moscow, Russia

<sup>7</sup>Biology Department, MSU-BIT University, Shenzhen, China

## Correspondence

Olga S. Sokolova, Lomonosov Moscow State University, Moscow 119234, Russia.  
Email: sokolova@mail.bio.msu.ru

## Funding information

Ministry of Science and Higher Education of the Russian Federation, Grant/Award Number: AAAA-A20-120081790043-5; Russian Foundation for Basic Research, Grant/Award Number: 20-04-60258

Review Editor: Alberto Diaspro

## Abstract

The severe COVID-19 pandemic drives the research toward the SARS-CoV-2 virion structure and the possible therapies against it. Here, we characterized the  $\beta$ -propiolactone inactivated SARS-CoV-2 virions using transmission electron microscopy (TEM) and atomic force microscopy (AFM). We compared the SARS-CoV-2 samples purified by two consecutive chromatographic procedures (size exclusion chromatography [SEC], followed by ion-exchange chromatography [IEC]) with samples purified by ultracentrifugation. The samples prepared using SEC and IEC retained more spikes on the surface than the ones prepared using ultracentrifugation, as confirmed by TEM and AFM. TEM showed that the spike (S) proteins were in the pre-fusion conformation. Notably, the S proteins could be recognized by specific monoclonal antibodies. Analytical TEM showed that the inactivated virions retained nucleic acid. Altogether, we demonstrated that the inactivated SARS-CoV-2 virions retain the structural features of native viruses and provide a prospective vaccine candidate.

## KEYWORDS

AFM, COVID-19, S protein, SARS-CoV-2, TEM

## 1 | INTRODUCTION

The severe COVID-19 pandemic that started in December 2019 is caused by the severe acute respiratory syndrome coronavirus

2 (SARS-CoV-2), a member of the *Coronaviridae* family (Zhou et al., 2020). The SARS-CoV-2 virion consists of a 30 kb positive-sense single-stranded RNA (ssRNA), bound with the nucleocapsid N protein and surrounded by a lipid membrane

with the embedded glycoprotein S and the transmembrane proteins M and E.

The glycoprotein S forms trimer spikes on the virion surface and determines the first stages of viral infection of the cell. The structure of the S protein ectodomain of the SARS-CoV-2 coronavirus was rapidly solved in February 2020 using cryo-electron microscopy at a resolution of 3.5 Å (Wrapp et al., 2020). The S protein molecule is subdivided into an S1 subunit (about 70 kDa), which binds to the ACE2 receptor via the receptor-binding domain (RBD) and the S2 subunit (about 60 kDa), which drives the fusion of the host and virion membranes. Structural studies (Yan et al., 2020; Lan et al., 2020) have confirmed the conserved nature of the SARS-CoV and SARS-CoV-2 epitopes and demonstrated that the RBD (CTD1) is bound in an “open” conformation to the ACE2 molecule (Yuan et al., 2020).

More than three million deaths were claimed by COVID-19 by May 2021, justifying the urgent widespread vaccination campaigns (World Health Organization, 2021). By the beginning of 2021, 213 candidate vaccines were in development worldwide, and 44 were in large-scale clinical trials; of those, eight were authorized for emergency use at least by one country's governing body. These include mRNA, adenovirus vector, inactivated, and peptide vaccines (Zhao et al., 2020). A traditional approach of inactivated vaccine development remains relatively simple, cost-efficient, and very promising, due to its successful history of use. Several inactivated vaccines against SARS-CoV-2 have been developed around the world, some of them showing success in clinical trials, which has led to their approval and use for vaccination in certain countries (Zhao et al., 2020). They appear to cause milder side effects than vector and mRNA vaccines (Carli, Nichele, Ruggeri, Barra, & Tosetto, 2021; Fernández-Prada, Rivero-Calle, Calvache-González, & Martín-Torres, 2021; Ndeupen et al., 2021).

Most vaccines exploit the S protein and RBD as the major antigens eliciting neutralizing antibodies and cellular response against SARS-CoV-2, although this choice is controversial. For instance, the nucleocapsid N protein can induce antibody production (Smits et al., 2021) as well as elicit broad-based cellular immune responses (Zhao et al., 2005), which may prevent infection. On the other hand, S protein is more prone to mutations than the other virion proteins (van Dorp et al., 2020), undermining the protection induced by S protein or RBD-based vaccines. Therefore, whole-virion vaccines, inducing more complex immune responses, may be more sustainable upon the SARS-CoV-2 evolutionary changes.

The structure of inactivated SARS-CoV-2 virions is crucial for the development of vaccine-induced immune response. Virus particle structure can be altered by the production process. Transmission electron microscopy (TEM) is routinely used as a general assessment method in situations where the speed of diagnostics is critical or where the diagnosis remains unclear even after the first analysis by alternative screening techniques (De Carlo & Harris, 2011). The key method here is negative staining; it is robust, well-established, and highly reproducible. The main advantages of negative staining EM are speed and high contrast. Identification of viruses by negative stain TEM is based on morphological criteria allowing the assignment of

viruses to a morphological group, which usually corresponds to a virus family (Goldsmith & Miller, 2009). In contrast, atomic force microscopy (AFM) is a less popular method for the investigation of viruses (Baclayon, Wuite, & Roos, 2010; de Pablo, 2019; Kuznetsov & McPherson, 2011). It is advantageous in two specific types of experiments—measurement of mechanical properties for individual virions and measurement of cell-virus interactions. Regular high-resolution AFM imaging both in the air and in the liquid may also bring valuable structural information (Kiss, Kis, Pályi, & Kellermayer, 2021).

Here, we present a thorough AFM and TEM characterization of the  $\beta$ -propiolactone-inactivated SARS-CoV-2 virions. The studied virion samples demonstrated the major structural features of the native viruses, supporting their consideration as prospective vaccine candidates.

## 2 | MATERIALS AND METHODS

### 2.1 | Preparation of the virus samples

SARS-CoV-2 vaccine strain AYDAR-1 (EPI ISL 428851) was isolated in Russia (Kozlovskaya et al., 2020). The virus was propagated in Vero cells on microcarriers and subjected to  $\beta$ -propiolactone (1:1000–1:2000, v/v) inactivation for 24–48 hr. Virus samples were then purified and concentrated via chromatography or ultracentrifugation.

For chromatography, the inactivated virus was cleared via ultrafiltration and diafiltration, followed by size exclusion chromatography (SEC) and ion-exchange chromatography (IEC). SEC was done using a HiScale 26/40 column (GE Healthcare, Chicago, IL) containing Sephacryl 6FF (Sunresin, Xi'an, China); for IEC—a HiScale 26/40 column containing the positively charged Capto DEAE matrix (GE Healthcare). The virus was eluted using an AKTA purifier (GE Healthcare) for SEC and AKTA pure 150M (GE Healthcare) for IEC, in a phosphate buffer in both cases.

For ultracentrifugation, the inactivated virus was centrifuged at 25000 rpm in the SW-28 rotor equipped Beckman ultracentrifuge. The pellets were resuspended in PBS and centrifuged through 10–50% sucrose gradient at 32000 rpm in the SW-40 rotor equipped Beckman ultracentrifuge for 4 hr at 4°C. Fractions were collected and analyzed by Ponceau staining. The most concentrated samples were transferred to HiTrap desalting columns for changing the sucrose solution to PBS.

Samples' purity was estimated using SDS-PAGE. The presence of SARS-CoV-2 N and S proteins in the samples was confirmed by Western blot with COVID-19 convalescent serum.

### 2.2 | Monoclonal antibodies preparation

Mouse monoclonal antibodies (mAbs) to SARS-CoV-2 were obtained using standard hybridoma technology. In brief, BALB/c mice were immunized with a recombinant RBD purified on Ni-NTA agarose (Qiagen, Hilden, Germany) from an *Escherichia coli* expression system.

Clones were selected by indirect ELISA with recombinant RBD expressed in HEK293 cells, as well as with ultraviolet-inactivated SARS-CoV-2 virus concentrate.

## 2.3 | TEM grids preparation

The carbon-coated TEM copper grids (Ted Pella, Redding, CA) were treated using a glow discharge device Emitech K100X (Quorum Technologies, Great Britain, England). Virus samples were diluted with phosphate-buffered saline (PBS), and 3–4 grids were prepared for each sample to achieve a convenient surface density of the adsorbed particles; 3  $\mu$ l of the sample was deposited onto the glow-discharged grids for 30 s. Then, the grids were immediately stained with 2% uranyl acetate or 2%  $(\text{NH}_4)_2\text{MoO}_4$  (for analytical studies) for 1 min and air-dried.

To investigate the interaction between the virions and antibodies, the grids with virus samples were incubated with mAb against RBD (770  $\mu$ g/ml) before staining.

## 2.4 | TEM and analytical electron microscopy

TEM images were obtained using the JEOL JEM-2100 LaB6 transmission electron microscope (JEOL, Akishima, Japan), operating at 200 kV with 40,000 $\times$  magnification and defocus  $-1.9 \mu\text{m}$ . In total, 33 samples were investigated, of which 25 were purified using chromatography, and eight samples were purified using ultracentrifugation. Overall, more than 150 photographs were collected and compared.

Electron microscopy was performed with the JEM-2100 200 kV LaB6 transmission electron microscope (JEOL) equipped with a Gatan GIF Quantum ER energy filter (Gatan, Pleasanton, CA) operating in spectrometer mode, along with a high-angle annular dark-field (HAADF) scanning TEM (STEM) detector. The cooling holder model 21,090 (JEOL) was operated at  $-182 \text{ }^\circ\text{C}$  to reduce the contamination effects and to enhance the specimen's stability under the electron beam. The microscope was operated in STEM mode with a 5 nm probe size and a 6 mrad spectrometer collection angle. Spectrum data for elemental mapping were collected with 0.25 eV/channel energy dispersion with 2048 detector channels, with 6 nm STEM pixel size, 0.2 s dwelling time, and summation over five frames. The spectrum data were aligned by carbon K peak at 283 eV. The background was extrapolated with power law over a 118–128 eV window; the signal window for phosphorus mapping was set to a 132–155 eV phosphorus L2, three peak range. No multiple scattering correction was applied.

## 2.5 | Atomic force microscopy

Freshly cleaved mica sheets were treated with 5 mM  $\text{NiCl}_2$  for 2 min, rinsed in MilliQ water, and dried. Then, sheets were treated with virus samples for 3–4 min, rinsed in MilliQ water, and dried. The AFM

measurements were carried out using a Solver Pro atomic force microscope (NT-MDT, Zelenograd, Russia). The scanning was carried out in semicontact mode and phase contrast mode using SSS-FMR cantilevers (Nanosensors, Neuchâtel, Switzerland; the tip curvature radius  $< 5 \text{ nm}$ ). The AFM images were processed using the Femtoscan online software package (Yaminsky, Filonov, Sinitsyna, & Meshkov, 2016).

## 3 | RESULTS AND DISCUSSION

### 3.1 | Chromatographically purified inactivated virus particles possess morphology, characteristic to native virions

Vaccines based on physically or chemically inactivated viruses have been successfully used to prevent poliomyelitis, rabies, hepatitis A, tick-borne encephalitis, and influenza (Gomez & Robinson, 2018). The antibodies induced by the inactivated virus particles had a better reactivity and specificity than those of the antibodies induced by the purified proteins (Liu et al., 2018).

Here, we used TEM and AFM to analyze the inactivated SARS-CoV-2 particles in the course of the inactivated vaccine development; we aimed to demonstrate that they retained characteristic structural features of the native viruses. When examined with TEM, the inactivated SARS-CoV-2 particles were roughly spherical (Figure 1a,b). Most virions adopted the “cup-shaped” morphology, typical for extracellular vesicles (Théry, Amigorena, Raposo, & Clayton, 2006) and large viruses, such as avian H5N8 influenza (Korneev, Kurskaya, Sharshov, Eastwood, & Strakhovskaya, 2019) and varicella-zoster virus (Buckingham, Jarosinski, Jackson, Carpenter, & Grose, 2016). This effect could arise due to two key factors—deformation of the viruses upon drying and penetration of uranyl acetate into the virions.

In the AFM images, the surface of virions was rough and consisted of globules and “tufts” similar to the previously described murine leukemia virus (Kuznetsov, Low, Fan, & McPherson, 2004). Previously, AFM imaging of individual SARS-CoV-2 S protein molecules on the virion surface was performed only in liquid (Kiss et al., 2021). Our experimental procedure exploits scanning in the air; it is relatively simple and can be further used for the analysis of the surface of various coronaviruses and their stability.

Up to 10% of particles were damaged, according to both TEM and AFM. This is a common problem encountered during virus preparation for microscopical studies (Kuznetsov et al., 2004). Nevertheless, both AFM and TEM revealed that the spikes on the surface of 90% of virions remained intact (Figure 1a,b). In our AFM study, the spikes were especially notable in the phase images (Figure 1c), which were often more sensitive to local structural features than the height images (Stark, Möller, Müller, & Guckenberger, 2001). The typical thickness of the corona in AFM was  $16 \pm 4 \text{ nm}$  (from this point onward, we report the data as the mean  $\pm$  SD), in agreement with the previous data obtained using AFM in liquid (Kiss et al., 2021).

### 3.2 | Spike structure in the inactivated virus particles resembles a pre-fusion conformation

The S glycoprotein is the most prominent feature of the coronavirus virion surface and is crucial for the first stages of virus entry into the cell. S protein is a typical class-I fusion protein: it forms a trimer, with each monomer consisting of a massive ectodomain, transmembrane, and short cytoplasmic domains (Jurazek et al., 2021; Ke et al., 2020; Turoňová et al., 2020; Yao et al., 2020). The “pre-fusion” ectodomain is cleaved by the host proteases into the S1 subunit (about 70 kDa), which binds to the receptor via the RBD, and the S2 subunit (about 60 kDa), which induces the fusion of host and virus membranes. After cleavage, the two subunits dissociate; S1 remains bound to the receptor and leaves (Song, Gui, Wang, & Xiang, 2018), whereas S2 undergoes a substantial conformational rearrangement, attacks the host cell lipid bilayer, induces the fusion of viral and cellular membranes, and transitions to the “post-fusion” state (McCallum, Walls, Bowen, Corti, & Veesler, 2020). It has been shown that only antibodies targeting the S protein can neutralize the virus and prevent infection (Jiang, Hillyer, & Du, 2020).

We employed TEM to measure the size and reveal the state of the S protein in the inactivated virions. The S protein spikes on the surface of the virions were  $15 \pm 2$  nm long and  $8 \pm 2$  nm wide, consistent with the pre-fusion state (Figure 2a), in a perfect agreement with the AFM data described above. AFM measurements in liquid yielded the height of individual S proteins of  $13 \pm 5$  nm (Kiss et al., 2021).

Images of inactivated virions were compared to those incubated with mAbs (Figure 2). The binding of the anti-RBD mAb to the S protein (Figure 2b,c) was observed around the distal end of the spikes, where the RBD was presumably located (Jurazek et al., 2021). We compared the intensity profiles (Figure 2e) along the sections across an ordinary virion (Figure 2d) and the one incubated with mAbs (Figure 2f). A single peak about 20 nm thick (marked with “S” on Figure 2e) was present in both images and, apparently, corresponded to the S protein density. In the virus samples treated with mAbs, an additional electron density region was observed, but it was absent in the non-treated ones. This density most likely corresponded to an mAb molecule bound to a virion. Moreover, this additional density

only appeared in contact with the S protein spikes, whereas the virion surfaces lacking spikes (Figure 2f) were not surrounded by the additional density. Therefore, the specific binding of mAb only to RBD and not to the other parts of the virion surface was confirmed.

### 3.3 | Phosphorus mapping using electron energy loss spectroscopy

Next, we performed electron energy loss spectroscopy (EELS) experiments to verify the presence of phosphorus (P) inside the virions. For these experiments, we used a negative stain with 2%  $(\text{NH}_4)_2\text{MoO}_4$ , rather than uranyl acetate, since the uranium O<sub>4</sub> five peak (edge at 96 eV) is close to the P L<sub>2</sub>, three peak (edge at 132 eV) and interferes with the accurate background interpolation. The typical distribution of P within a single virion is shown in Figure 3a. The intensity under the P peak after the background subtraction was used for STEM-EELS mapping. We observed the characteristic P signal from the inner part of the virion but not from the bare grid (Figure 3b). The observed P signal could arise either from the viral RNA or the lipids of the virus membrane, and since the P signal was highly heterogeneous, it was more likely to originate from the RNA. The spatial distribution and intensity of the P signal differed significantly (Figure 3a, insert). This clearly reflected a non-even distribution of the genomic RNA, which apparently accompanied virions' inner heterogeneity, previously observed by in-situ cryo-electron tomography (Klein et al., 2020). Authors suggested that the large coronavirus genome was partially associated with the N protein forming multiple vRNPs, which enables their steric separation.

So far, phosphorus mapping in individual virions using EELS was performed only on the samples prepared using highly specialized techniques, which minimized the sample thickness, including the substrate thickness. For example, P mapping was described for free-standing films made of the  $\lambda$  bacteriophage (Nevsten, Evilevitch, & Wallenberg, 2012) or ultrathin sections of murine leukemia viruses (Ottensmeyer & Andrew, 1980). These experiments relied on energy-filtered TEM (EFTEM), which seems to be more prone to artifacts than STEM-EELS used in the current study. The heterogeneity of the

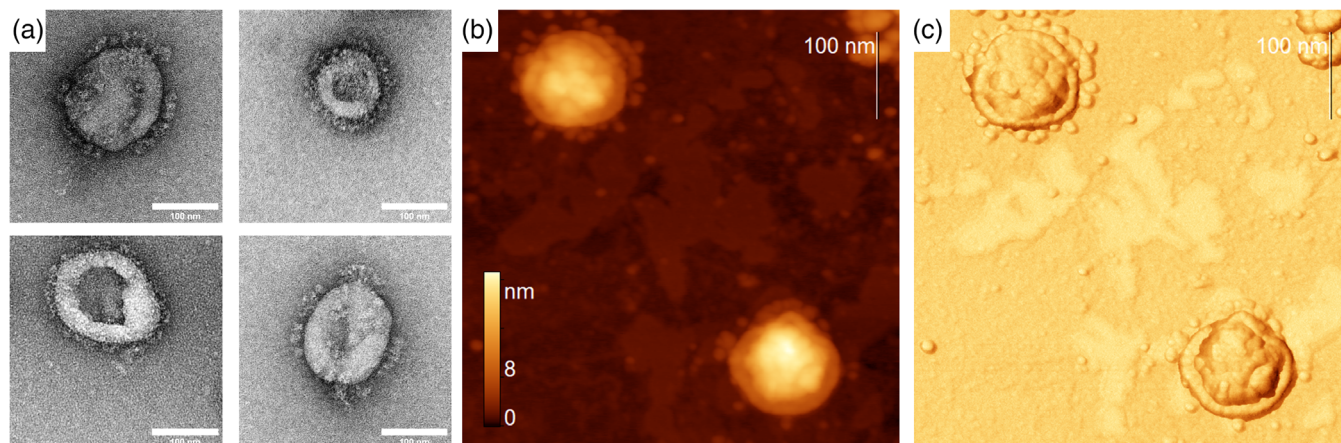


**FIGURE 1** Images of the purified corona-bearing virus particles visualized by (a) TEM and (b,c) AFM—(b) height image and (c) phase image

nucleic acid inside the virions was also demonstrated for flaviviruses (Moiseenko et al., 2021; Rey, Stiasny, & Heinz, 2017).

### 3.4 | The purification technique affects the morphology of the virus particles

Finally, we compared the methods of virus sample purification. The sizes of the virions in the TEM images were measured using the

ScanEV online tool (Nikishin et al., 2021). Histograms of size distributions are presented in Figure 4c. Ultracentrifugation (UC) yielded more monodisperse and pure samples (mean size  $D_{UC\ TEM} = 103 \pm 11$  nm) than chromatography ( $D_{SEC+IEC\ TEM} = 107 \pm 29$  nm). The difference in size variations was statistically significant, according to the F-test for variances ( $p = 6.7 \times 10^{-12}$ ). When the virions were prepared using ultracentrifugation, their size distribution was relatively narrow; the images showed fewer large particles and almost no debris. The size heterogeneity of individual virions could be an intrinsic

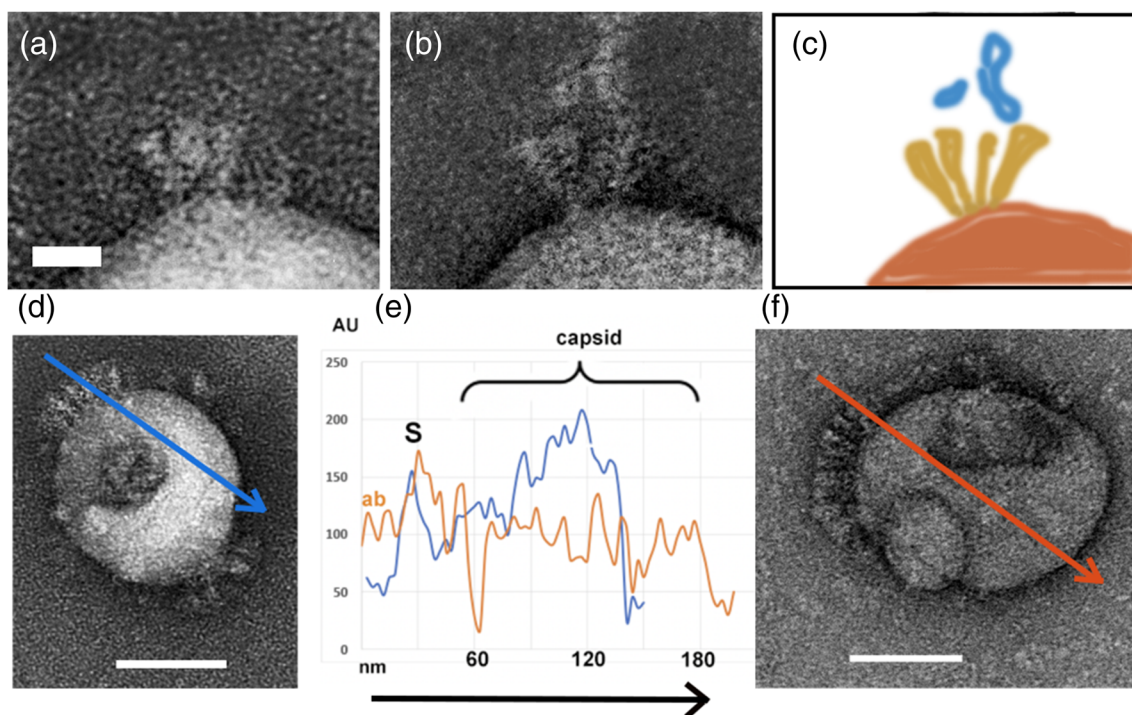


**FIGURE 2** Antibody labeling of the S protein on the virions. Raw images of the S proteins (a) on the surface of inactivated SARS-CoV-2 virions, bar size—20 nm. (b) After incubation with mAb. (c) Schematic, illustrating a raw image in (b): antibody—blue; S proteins—yellow; capsid—orange. (d) Control virion. (f) Virion after incubation with mAb, bar size—50 nm. (e) Intensity profiles across the lines in (d,f), superimposed. Colors in (e) correspond to the line colors in (d,f). The black arrow at the bottom of the graph shows the direction of the intensity profile's reading. “S” marks the intensity that corresponds to the S-proteins. ab—density, corresponding to a bound mAb molecule

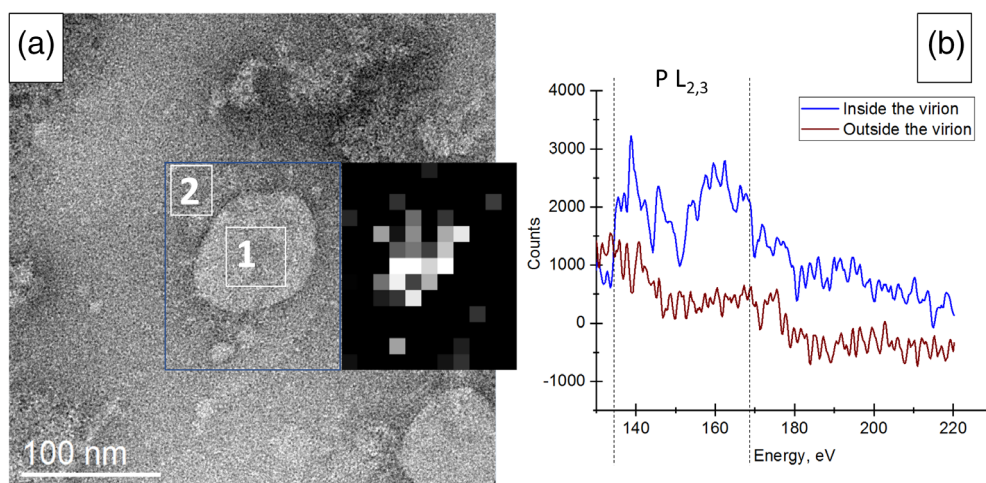


**FIGURE 3** (a) TEM image of the virus particle with area for EELS spectrum acquisition and corresponding elemental mapping. The phosphorus distribution map reveals the localization of phosphorus inside the particle (region 1), but not outside (region 2). (b) EELS spectra acquired in STEM mode and summed over areas of interest (1 and 2) shown in (a)

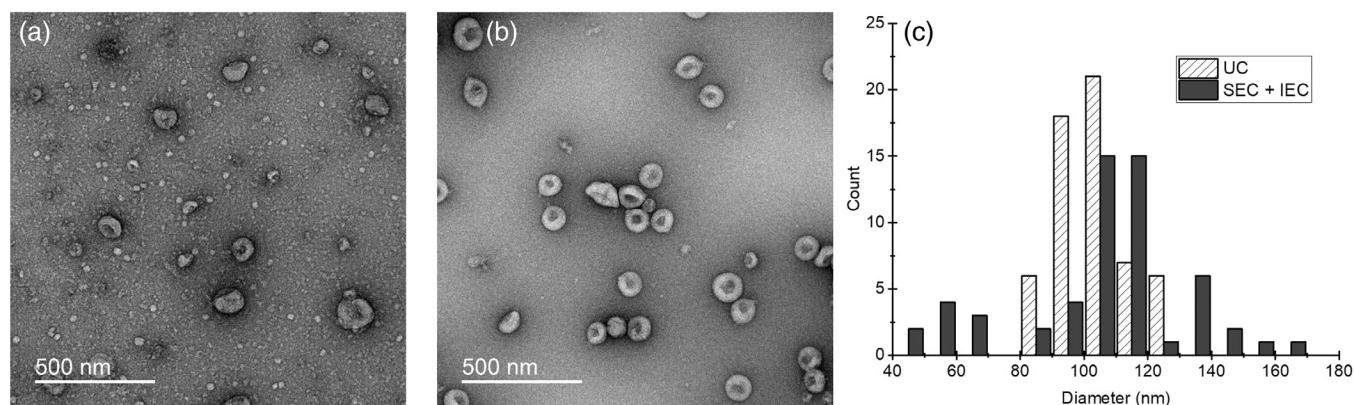


**FIGURE 4** TEM images of SARS-CoV-2 virions purified using (a) SEC + IEC and (b) ultracentrifugation. (c) Distributions of virion diameter, depending on the purification method

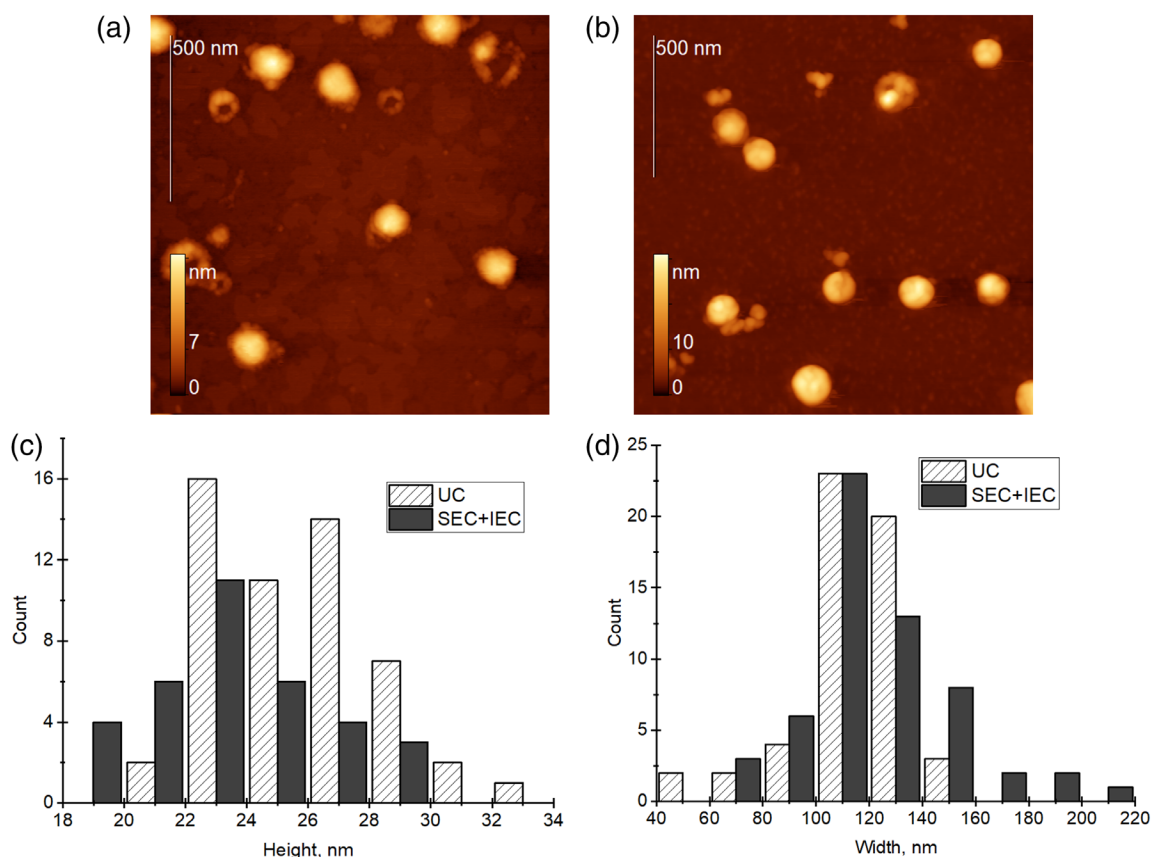


**FIGURE 5** AFM images of SARS-CoV-2 virions purified using (a) chromatography and (b) ultracentrifugation. The histograms of the (c) height distributions and (d) width distributions

property of the virus, as shown for flaviviruses (Rey et al., 2017) and HIV (Pang, Song, Kim, Hou, & Cheng, 2014). Chromatography allowed to retain the S protein spikes on most particles (Figure 4a), whereas only a few ultracentrifugation-purified virions retained the spikes on the surface (Figure 4b).

AFM images of the virions prepared using two purification methods are shown in Figure 5a,b. The height of the particles was  $h_{\text{SEC + IEC}} = 24 \pm 3$  nm and  $h_{\text{UC}} = 25 \pm 3$  nm for the samples purified

using SEC + IEC and ultracentrifugation, respectively (Figure 5c). The height was far lower than the diameter measured using TEM, and the difference indicated a flattening deformation of the virions on the mica surface. When imaged in liquid, the mean height of the virions was 83 nm (Kiss et al., 2021). In agreement with the TEM observations, AFM showed that the samples purified using ultracentrifugation were relatively homogeneous in their lateral size (Figure 5d). The width of individual virions was  $D_{\text{UC AFM}} = 114 \pm 20$  nm and  $D_{\text{SEC + IEC}}$

$A_{FM} = 127 \pm 27$  nm. These values were larger than the ones measured using TEM due to the tip broadening effect. In agreement with the TEM data, the virions purified using SEC + IEC were more heterogeneous than the ones purified using ultracentrifugation.

## 4 | CONCLUSIONS

SARS-CoV-2 is a Risk Group 3 pathogen, implying specific requirements on laboratory biosafety measures and personnel training (Kaufer, Theis, Lau, Gray, & Rawlinson, 2020). Many biological laboratories, which could contribute to the struggle against the pandemic, are unable to fulfill these requirements. However, they can handle the inactivated virus and make valuable conclusions if the inactivated model captures the fundamental properties of the active virus. Here, we analyzed the properties of the  $\beta$ -propiolactone inactivated virions and demonstrated that they retained the key structural features of the native viruses.

Purification of SARS-CoV-2 virions could be performed in two major ways, chromatography and ultracentrifugation. Whereas the latter appeared to provide more uniform and pure inactivated virion particles, chromatography led to the acquisition of samples with more intact S protein spikes on the virion surface. Chromatography remains the method of choice for vaccine production, whereas ultracentrifugation can be used for pure sample preparation for structural studies. Here, we demonstrated, using TEM and AFM, that the chromatography purification method led to the preservation of the S protein spikes on the virion surface, which, in turn, could be recognized by the specific antibodies. The presence of RNA inside the virions was demonstrated using STEM-EELS based on the phosphorus signal. The virus inactivation and purification procedures described in the current work were adopted in the production of the CoviVac vaccine (Kozlovskaya et al., 2021), which is currently in the phase III of clinical trials.

## ACKNOWLEDGMENTS

The authors thank Lisa Trifonova for proof-reading the manuscript. Electron microscopy was performed at the scientific facility “3D Electron Microscopy and Spectroscopy” of the Department of Biology, Lomonosov Moscow State University. Mikhail P. Kirpichnikov, Konstantin V. Shaitan, Dmitry V. Bagrov, and Olga S. Sokolova acknowledge the support from the Interdisciplinary Scientific and Educational School of Lomonosov Moscow State University “Molecular Technologies of the Living Systems and Synthetic Biology” as part of the Scientific Project of the State Order of the Government of the Russian Federation to Lomonosov Moscow State University No. 121032500056-3.

## ORCID

Dmitry V. Bagrov  <https://orcid.org/0000-0002-6355-7282>

Liubov I. Kozlovskaya  <https://orcid.org/0000-0002-3029-1035>

Dmitry I. Osolodkin  <https://orcid.org/0000-0002-0462-2945>

Aydar A. Ishmukhametov  <https://orcid.org/0000-0001-6130-4145>

Konstantin V. Shaitan  <https://orcid.org/0000-0002-5137-303X>

Olga S. Sokolova  <https://orcid.org/0000-0003-4678-232X>

## REFERENCES

- Baclayon, M., Wuite, G. J. L., & Roos, W. H. (2010). Imaging and manipulation of single viruses by atomic force microscopy. *Soft Matter*, 6, 5273. <https://doi.org/10.1039/b923992h>
- Buckingham, E. M., Jarosinski, K. W., Jackson, W., Carpenter, J. E., & Grose, C. (2016). Exocytosis of varicella-zoster virus virions involves a convergence of endosomal and autophagy pathways. *Journal of Virology*, 90, 8673–8685. <https://doi.org/10.1128/jvi.00915-16>
- Carli, G., Nichele, I., Ruggeri, M., Barra, S., & Tosetto, A. (2021). Deep vein thrombosis (DVT) occurring shortly after the second dose of mRNA SARS-CoV-2 vaccine. *Internal and Emergency Medicine*, 16, 803–804. <https://doi.org/10.1007/s11739-021-02685-0>
- De Carlo, S., & Harris, J. R. (2011). Negative staining and cryo-negative staining of macromolecules and viruses for TEM. *Micron*, 42, 117–131. <https://doi.org/10.1016/j.micron.2010.06.003>
- de Pablo, P. J. (2019). The application of atomic force microscopy for viruses and protein shells: Imaging and spectroscopy. In F. A. Rey (Ed.), *Complementary strategies to understand virus structure and function Advances in virus research* (pp. 161–187). Cambridge, MA: Academic Press. <https://doi.org/10.1016/bs.aivir.2019.07.006>
- Fernández-Prada, M., Rivero-Calle, I., Calvache-González, A., & Martín-Torres, F. (2021). Acute onset supraclavicular lymphadenopathy coinciding with intramuscular mRNA vaccination against COVID-19 may be related to vaccine injection technique, Spain, January and February 2021. *Eurosurveillance*, 26(10):2100193. <https://doi.org/10.2807/1560-7917.ES.2021.26.10.2100193>
- Goldsmith, C. S., & Miller, S. E. (2009). Modern uses of electron microscopy for detection of viruses. *Clinical Microbiology Reviews*, 22, 552–563. <https://doi.org/10.1128/CMR.00027-09>
- Gomez, P. L., & Robinson, J. M. (2018). Vaccine manufacturing. In *Plotkin's vaccines* (pp. 51–60.e1). Amsterdam, Netherlands: Elsevier Inc. <https://doi.org/10.1016/b978-0-323-35761-6.00005-5>
- Jiang, S., Hillyer, C., & Du, L. (2020). Neutralizing antibodies against SARS-CoV-2 and other human coronaviruses. *Trends in Immunology*, 41, 355–359. <https://doi.org/10.1016/j.it.2020.03.007>
- Juraszek, J., Rutten, L., Blokland, S., Bouchier, P., Voorzaat, R., Ritschel, T., ... Langedijk, J. P. M. (2021). Stabilizing the closed SARS-CoV-2 spike trimer. *Nature Communications*, 12, 244. <https://doi.org/10.1038/s41467-020-20321-x>
- Kaufer, A. M., Theis, T., Lau, K. A., Gray, J. L., & Rawlinson, W. D. (2020). Laboratory biosafety measures involving SARS-CoV-2 and the classification as a Risk Group 3 biological agent. *Pathology*, 52, 790–795. <https://doi.org/10.1016/j.pathol.2020.09.006>
- Ke, Z., Oton, J., Qu, K., Cortese, M., Zila, V., McKeane, L., ... Briggs, J. A. G. (2020). Structures and distributions of SARS-CoV-2 spike proteins on intact virions. *Nature*, 588, 498–502. <https://doi.org/10.1038/s41586-020-2665-2>
- Kiss, B., Kis, Z., Pályi, B., & Kellermayer, M. S. Z. (2021). Topography, spike dynamics, and nanomechanics of individual native SARS-CoV-2 virions. *Nano Letters*, 21, 2675–2680. <https://doi.org/10.1021/acs.nanolett.0c04465>
- Klein, S., Cortese, M., Winter, S. L., Wachsmuth-Melm, M., Neufeldt, C. J., Cerikan, B., ... Chlanda, P. (2020). SARS-CoV-2 structure and replication characterized by in situ cryo-electron tomography. *Nature Communications*, 11, 5885. <https://doi.org/10.1038/s41467-020-19619-7>
- Korneev, D., Kurskaya, O., Sharshov, K., Eastwood, J., & Strakhovskaya, M. (2019). Ultrastructural aspects of photodynamic inactivation of highly pathogenic avian H5N8 influenza virus. *Viruses*, 11, 1–11. <https://doi.org/10.3390/v11100955>
- Kozlovskaya, L., Pinaeva, A., Ignatyev, G., Selivanov, A., Shishova, A., Kovpak, A., ... Ishmukhametov, A. (2020). Isolation and phylogenetic analysis of SARS-CoV-2 variants collected in Russia during the COVID-19 outbreak. *International Journal of Infectious Diseases*, 99, 40–46. <https://doi.org/10.1016/j.ijid.2020.07.024>
- Kozlovskaya, L. I., Pinaeva, A. N., Ignatyev, G. M., Gordeychuk, I. V., Volok, V. P., Rogova, Y. V., ... Ishmukhametov, A. A. (2021). Long-term

- humoral immunogenicity, safety and protective efficacy of inactivated vaccine against COVID-19 (CoviVac) in preclinical studies. *Emerging Microbes & Infections*, 10. in press. <https://doi.org/10.1080/22221751.2021.1971569>
- Kuznetsov, Y. G., Low, A., Fan, H., & McPherson, A. (2004). Atomic force microscopy investigation of wild-type Moloney murine leukemia virus particles and virus particles lacking the envelope protein. *Virology*, 323, 189–196. <https://doi.org/10.1016/j.virol.2004.02.023>
- Kuznetsov, Y. G., & McPherson, A. (2011). Atomic force microscopy in imaging of viruses and virus-infected cells. *Microbiology and Molecular Biology Reviews*, 75, 268–285. <https://doi.org/10.1128/mmr.00041-10>
- Kuznetsov, Y. G., Victoria, J. G., Low, A., Robinson, W. E., Fan, H., & McPherson, A. (2004). Atomic force microscopy imaging of retroviruses: Human immunodeficiency virus and murine leukemia virus. *Scanning*, 26, 209–216. <https://doi.org/10.1002/sca.4950260409>
- Lan, J., Ge, J., Yu, J., Shan, S., Zhou, H., Fan, S., ... Wang, X. (2020). Structure of the SARS-CoV-2 spike receptor-binding domain bound to the ACE2 receptor. *Nature*, 581, 215–220. <https://doi.org/10.1038/s41586-020-2180-5>
- Liu, X., Ouyang, T., Ma, T., Ouyang, H., Pang, D., & Ren, L. (2018). Immunogenicity evaluation of inactivated virus and purified proteins of porcine circovirus type 2 in mice. *BMC Veterinary Research*, 14, 137. <https://doi.org/10.1186/s12917-018-1461-9>
- McCallum, M., Walls, A. C., Bowen, J. E., Corti, D., & Velesler, D. (2020). Structure-guided covalent stabilization of coronavirus spike glycoprotein trimers in the closed conformation. *Nature Structural & Molecular Biology*, 27, 942–949. <https://doi.org/10.1038/s41594-020-0483-8>
- Moiseenko A., Zaitsev P., Vorovitch M., Osolodkin D., Ishmukhametov A., Egorov A., Shaitan K. V., Kirpichnikov M. P., & Sokolova O. S. (2021). Estimation of the structural heterogeneity of Tick-Borne Encephalitis vaccine particles. *Microscopy and Microanalysis*. 27:(S1), 84–86. <http://doi.org/10.1017/s1431927621000921>
- Ndeupen, S., Qin, Z., Jacobsen, S., Gibb, M., Estabouli, H., Bouteau, A., ..., Igyarto, B. Z., 2021. The mRNA-LNP platform's lipid nanoparticle component used in preclinical vaccine studies is highly inflammatory. *bioRxiv* March 4, 2021. 430128. <https://doi.org/10.1101/2021.03.04.430128>
- Nevsten, P., Evilevitch, A., & Wallenberg, R. (2012). Chemical mapping of DNA and counter-ion content inside phage by energy-filtered TEM. *Journal of Biological Physics*, 38, 229–240. <https://doi.org/10.1007/s10867-011-9234-8>
- Nikishin, I., Dulimov, R., Skryabin, G., Galetsky, S., Tchevkina, E., & Bagrov, D. (2021). ScanEV – A neural network-based tool for the automated detection of extracellular vesicles in TEM images. *Micron*, 145, 103044. <https://doi.org/10.1016/j.micron.2021.103044>
- Ottensmeyer, F. P., & Andrew, J. W. (1980). High-resolution microanalysis of biological specimens by electron energy loss spectroscopy and by electron spectroscopic imaging. *Journal of Ultrastructure Research*, 72, 336–348. [https://doi.org/10.1016/S0022-5320\(80\)90069-6](https://doi.org/10.1016/S0022-5320(80)90069-6)
- Pang, Y., Song, H., Kim, J. H., Hou, X., & Cheng, W. (2014). Optical trapping of individual human immunodeficiency viruses in culture fluid reveals heterogeneity with single-molecule resolution. *Nature Nanotechnology*, 9, 624–630. <https://doi.org/10.1038/nnano.2014.140>
- Rey, F. A., Stiasny, K., & Heinz, F. X. (2017). Flavivirus structural heterogeneity: Implications for cell entry. *Current Opinion in Virology*, 24, 132–139. <https://doi.org/10.1016/j.coviro.2017.06.009>
- Smits, V. A. J., Hernández-Carralero, E., Paz-Cabrera, M. C., Cabrera, E., Hernández-Reyes, Y., Hernández-Fernaud, J. R., ... Freire, R. (2021). The Nucleocapsid protein triggers the main humoral immune response in COVID-19 patients. *Biochemical and Biophysical Research Communications*, 543, 45–49. <https://doi.org/10.1016/j.bbrc.2021.01.073>
- Song, W., Gui, M., Wang, X., & Xiang, Y. (2018). Cryo-EM structure of the SARS coronavirus spike glycoprotein in complex with its host cell receptor ACE2. *PLoS Pathogens*, 14, 1–19. <https://doi.org/10.1371/journal.ppat.1007236>
- Stark, M., Möller, C., Müller, D. J., & Guckenberger, R. (2001). From images to interactions: High-resolution phase imaging in tapping-mode atomic force microscopy. *Biophysical Journal*, 80, 3009–3018. [https://doi.org/10.1016/S0006-3495\(01\)76266-2](https://doi.org/10.1016/S0006-3495(01)76266-2)
- Théry C., Amigorena S., Raposo G., Clayton A.. Isolation and Characterization of Exosomes from Cell Culture Supernatants and Biological Fluids. *Current Protocols in Cell Biology*. 2006;30:(1):3–22. <http://dx.doi.org/10.1002/0471143030.cb0322s30>
- Turoňová, B., Sikora, M., Schürmann, C., Hagen, W. J. H., Welsch, S., Blanc, F. E. C., ... Beck, M. (2020). In situ structural analysis of SARS-CoV-2 spike reveals flexibility mediated by three hinges. *Science*, 370, 203–208. <https://doi.org/10.1126/science.abd5223>
- van Dorp, L., Acman, M., Richard, D., Shaw, L. P., Ford, C. E., Ormond, L., ... Balloux, F. (2020). Emergence of genomic diversity and recurrent mutations in SARS-CoV-2. *Infection, Genetics and Evolution*, 83, 104351. <https://doi.org/10.1016/j.meegid.2020.104351>
- World Health Organization (2021). WHO coronavirus disease (COVID-19) dashboard [WWW document]. URL <https://covid19.who.int/>
- Wrapp, D., Wang, N., Corbett, K. S., Goldsmith, J. A., Hsieh, C.-L., Abiona, O., ... McLellan, J. S. (2020). Cryo-EM structure of the 2019-nCoV spike in the prefusion conformation. *Science*, 367, 1260–1263. <https://doi.org/10.1126/science.abb2507>
- Yaminsky, I., Filonov, A., Sinitsyna, O., & Meshkov, G. (2016). FemtoScan online software. *Nanoindustry*, 2 (64):42–46. <https://doi.org/10.22184/1993-8578.2016.64.2.42.46>
- Yan, R., Zhang, Y., Li, Y., Xia, L., Guo, Y., & Zhou, Q. (2020). Structural basis for the recognition of SARS-CoV-2 by full-length human ACE2. *Science*, 367, 1444–1448. <https://doi.org/10.1126/science.abb2762>
- Yao, H., Song, Y., Chen, Y., Wu, N., Xu, J., Sun, C., ... Li, S. (2020). Molecular architecture of the SARS-CoV-2 virus. *Cell*, 183, 730–738.e13. <https://doi.org/10.1016/j.cell.2020.09.018>
- Yuan, M., Wu, N. C., Zhu, X., Lee, C.-C. D., So, R. T. Y., Lv, H., ... Wilson, I. A. (2020). A highly conserved cryptic epitope in the receptor binding domains of SARS-CoV-2 and SARS-CoV. *Science*, 368, 630–633. <https://doi.org/10.1126/science.abb7269>
- Zhao, J., Zhao, S., Ou, J., Zhang, J., Lan, W., Guan, W., ... Zhang, Q. (2020). COVID-19: Coronavirus vaccine development updates. *Frontiers in Immunology*, 11, 1–19. <https://doi.org/10.3389/fimmu.2020.602256>
- Zhao, P., Cao, J., Zhao, L.-J., Qin, Z.-L., Ke, J.-S., Pan, W., ... Qi, Z.-T. (2005). Immune responses against SARS-coronavirus nucleocapsid protein induced by DNA vaccine. *Virology*, 331, 128–135. <https://doi.org/10.1016/j.virol.2004.10.016>
- Zhou, P., Yang, X.-L., Wang, X.-G., Hu, B., Zhang, L., Zhang, W., ... Shi, Z.-L. (2020). A pneumonia outbreak associated with a new coronavirus of probable bat origin. *Nature*, 579, 270–273. <https://doi.org/10.1038/s41586-020-2012-7>

**How to cite this article:** Bagrov, D. V., Glukhov, G. S., Moiseenko, A. V., Karlova, M. G., Litvinov, D. S., Zaitsev, P. A., Kozlovskaya, L. I., Shishova, A. A., Kovpak, A. A., Ivin, Y. Y., Piniaeva, A. N., Oksanich, A. S., Volok, V. P., Osolodkin, D. I., Ishmukhametov, A. A., Egorov, A. M., Shaitan, K. V., Kirpichnikov, M. P., & Sokolova, O. S. (2022). Structural characterization of  $\beta$ -propiolactone inactivated severe acute respiratory syndrome coronavirus 2 (SARS-CoV-2) particles. *Microscopy Research and Technique*, 85(2), 562–569. <https://doi.org/10.1002/jemt.23931>